

Dipole Formation at Interfaces of Alkanethiolate Self-assembled Monolayers and Ag(111)

Paul C. Rusu,¹ Gianluca Giovannetti,^{2,1} and Geert Brocks^{1,*}

¹*Computational Materials Science, Faculty of Science and Technology and MESA+ Institute for Nanotechnology, University of Twente, P.O. Box 217, 7500 AE Enschede, The Netherlands*

²*Institute Lorentz for Theoretical Physics, Leiden University, P. O. Box 9506, 2300AE Leiden, The Netherlands.*

(Dated: November 11, 2018)

The formation of interface dipoles in self-assembled monolayers (SAMs) of $-\text{CH}_3$ and $-\text{CF}_3$ terminated short-chain alkanethiolates on Ag(111) is studied by means of density functional theory calculations. The interface dipoles are characterized by monitoring the change in the surface work function upon adsorption of the SAM. We compare results obtained for SAMs in structures with a different packing density of molecules, i.e. $(\sqrt{7} \times \sqrt{7})R19.1^\circ$, $(\sqrt{3} \times \sqrt{3})R30^\circ$, and $p(2 \times 2)$. The work function of alkanethiolate SAMs on silver depends weakly on the packing density; that of fluorinated alkanethiolates shows a stronger dependence. The results are analyzed in terms of two nearly independent contributions to the interface dipole. These originate respectively from the molecular dipoles and from a charge transfer between the metal surface and the molecules. The charge transfer is determined by the silver-sulfur bond and it is independent of the electronegativity of the molecules.

1. INTRODUCTION

Self-assembled monolayers (SAMs) of organothiolates on metal surfaces are studied for a wide range of technological applications running from catalysis, biosensors to microelectronic devices [1, 2, 3]. In organic light-emitting diodes, the interfaces between the metal contacts and the organic material are critical in the device performance, since they control the injection of electrons and holes into the device [4]. Chemisorption of a SAM on a metal surface can alter its work function substantially. Depending on the SAM, the work function can be manipulated advantageously to lower the energy barrier for electron and hole injection [5, 6, 7].

Self-assembled monolayers have also become attractive for fundamental studies in metal-organic interfaces and molecular electronics. They represent stable and ordered structures, which can be prepared experimentally in air, in solution, or in vacuum [8, 9]. SAMs of alkanethiolates, $\text{C}_n\text{H}_{2n+1}\text{S}$, on Au(111) are among the most extensively studied systems. Alkanethiolate SAMs on Au(111) adopt a $(\sqrt{3} \times \sqrt{3})R30^\circ$ structure or superstructures thereof [10, 11]. Alkanethiolates form SAMs on a wide range of (noble) metal surfaces, which have a similar structure as on Au(111). Variations on the packing density are possible, however, and on Ag(111) a somewhat denser packed $(\sqrt{7} \times \sqrt{7})R19.1^\circ$ structure has been reported [9].

The change in work function of the surface upon adsorption of the SAM is directly proportional to the dipole moment density generated at the SAM-metal interface. For SAMs on Au(111) it has been shown that this dipole moment density is mainly determined by the permanent

dipoles in the thiolate molecular layer. The sulfur-gold bonds that are formed upon adsorption, are nearly apolar and give a very small contribution to the interface dipole [12, 13, 14, 15]. However, a small sulfur-metal bond dipole is typical of gold and the existence of a much larger bond dipole is indicated by experiments of alkanethiolate SAMs on silver [7]. In a previous computational study on model structures we have shown that large bond dipoles can be formed in the adsorption of SAMs on Ag and Pt surfaces [16].

In this paper we study the interface dipole formation resulting from adsorption of SAMs on Ag(111) by first-principles density functional theory (DFT) calculations. In particular we examine the influence of the structure and the packing density of the molecules in the SAM. The $(\sqrt{7} \times \sqrt{7})R19.1^\circ$ packing, which is observed experimentally for alkanethiolate SAMs on Ag(111) [9], is our starting point. We consider several low energy structures [17, 18]. The results are compared to the $(\sqrt{3} \times \sqrt{3})R30^\circ$ structure, where the surface area per adsorbed molecule is 29% larger, which is the most common structure of alkanethiolate SAMs on other noble metal (111) surfaces. We also consider the less densely packed $p(2 \times 2)$ structure, which has a 71% higher surface area per molecule. Fluorinated alkanethiolate SAMs on Au(111) can be observed in this structure [9], and it might be possible that this structure is also formed by such molecules adsorbed on Ag(111). We show that although the interface dipole density is smaller for less densely packed structures, it is not simply proportional to the packing density due to dielectric screening in the molecular layer.

The commonly used DFT functionals describe the formation of chemical bonds and the resulting charge distribution very well, but they fail to capture the van der Waals interactions between the alkyl chains. Van der Waals interactions are relatively unimportant in short chain alkanethiolates, which is why we focus on the short

*Corresponding author; phone: 31-53-489-3155; fax: 31-53-489-2910; e-mail: g.h.l.a.brocks@tnw.utwente.nl.

chain thiols CH_3S and $\text{C}_2\text{H}_5\text{S}$. To elucidate the influence of the polarity of the molecules on the SAM–metal interface dipole, we also study the fluorinated thiols CF_3S and $\text{CF}_3\text{CH}_2\text{S}$. Since the directions of the dipole moment of fluorinated and of nonfluorinated thiols are roughly opposite, this leads to an obvious difference in the interface dipole between SAMs of the two types of molecules. In addition, fluorinated thiols have a much higher electronegativity. One would expect that by varying the relative electronegativity of the surface and the molecules, one can modify the electron transfer between surface and molecules, which would give an additional contribution to the interface dipole.

In this paper we will show that increasing the electronegativity by fluorinating the alkyl tails does however not lead to a change in charge transfer. We will arrive at this conclusion by analyzing the interface dipole and separating it into a contribution from the molecular dipoles and from the charge reordering at the metal–SAM interface. By comparing these results to those obtained for SAM–Au(111) and SAM–Pt(111) interfaces, it can be concluded that the charge transfer depends on the metal surface and the nature of the sulfur–metal bond, but not on the molecular tails.

The paper is organized as follows. In the next section we describe the techniques we use for calculating and analyzing the interface dipoles and give details on the parameters used in the calculations. Subsequently the results on the SAM–Ag(111) interfaces are discussed. First we discuss the possible structures and then we analyze the interface dipoles. The last section contains a short summary and the conclusions.

2. THEORETICAL SECTION

2.1. Total energy calculations

The Ag(111) metal surface is represented by a slab of layers of metal atoms stacked according to an *fcc* ABC sequence. A typical slab consists of four layers. The SAM is adsorbed on one side of the slab. The surface unit cell depends upon the monolayer structure and coverage. The cells used in our calculations are $(\sqrt{7} \times \sqrt{7})R19.1^\circ$, $(\sqrt{3} \times \sqrt{3})R30^\circ$, and $p(2 \times 2)$, which contain 7, 3 and 4 metal atoms per layer, respectively. Periodic boundary conditions are applied in all three directions. This means that not only are the cells repeated along the surface (the *xy*-plane), but also the slabs are repeated in the *z*-direction. The atoms in neighboring cells are separated along the *z*-direction by a vacuum region of ~ 12 Å. To cancel the artificial interaction between the dipoles of the repeated slabs, the Neugebauer-Scheffler dipole correction is applied [19].

The electronic structure is treated within density functional theory (DFT) [20] using the PW91 functional [21] to describe the electronic exchange and correlation. The calculations are performed with the program VASP (Vienna *ab initio* simulation package) [22, 23] using the pro-

jector augmented wave (PAW) method [24, 25]. For noble metal atoms the outer shell *s* and *d* electrons are treated as valence electrons, and for first and second row elements the outer shell *s* and *p* electrons. The valence pseudo wave functions are expanded in a basis set consisting of plane waves. All plane waves up to a kinetic energy cutoff of 500 eV are included.

The geometries are optimized by allowing the atoms in the top two metal layers and the atoms in the SAMs to relax. The (1×1) surface unit cell parameter is fixed at its optimized bulk value of 2.93 Å. The calculations use a **k**-point sampling mesh of 7×7 for the $(\sqrt{7} \times \sqrt{7})$ structure, 11×11 for the $(\sqrt{3} \times \sqrt{3})$ and 9×9 for the (2×2) structures, according to the Monkhorst-Pack scheme. For geometry optimization a Methfessel-Paxton smearing is used with a broadening parameter of 0.2 eV [26]. The energies of the optimized geometries are recalculated using the tetrahedron scheme [27]. Tests regarding the slab thickness, vacuum thickness, **k**-point sampling grid, and plane wave kinetic energy cutoff are performed, from which we estimate that total energy differences are converged to within ~ 0.05 eV.

The adsorption energy of the SAM is calculated by comparing the total energy of the slab (with the adsorbed SAM), with that of the clean slab (with the top surface in its relaxed Ag(111) structure), and the free alkanethiolate (radical) molecules. If SAM adsorption results in a reconstruction of the surface that involves metal adatoms [18, 28], we assume that these adatoms are supplied by the bulk metal. The adsorption energy per molecule E_{ads} associated with a surface structure that contains M molecules, N_s metal atoms per layer and N_{ad} adatoms is then given by

$$E_{\text{ads}} = \frac{1}{M} [E_{\text{slab}} - N_s E_{\text{clean}} - N_{\text{ad}} E_{\text{bulk}}] - E_{\text{mol}}, \quad (1)$$

where E_{slab} is the total energy of the slab, E_{clean} is the total energy of the clean slab per surface atom (top surface in optimized Ag(111) structure), E_{bulk} is the total energy of bulk Ag per atom, and E_{mol} is the total energy of an alkanethiolate molecule. Note that E_{ads} is negative if the adsorption is exothermic.

To analyze the results we have also calculated several properties of isolated thiolate molecules: dipole moments, ionization potentials, electron affinities and electronegativities. For these calculations we use the GAMESS program [29], and treat the electronic structure within DFT using the B3LYP functional [30, 31]. We use the aug-cc-pVTZ basis set. Calculations with the smaller 6-311G** basis set give dipole moments that are up to ~ 0.15 D smaller, and ionization potentials, electron affinities that differ by ~ 0.1 eV.

2.2. Work functions and interface dipoles

Interface dipoles can be extracted from the change in the surface work function upon adsorption of a SAM on a metal surface, as will be described below. Surface work

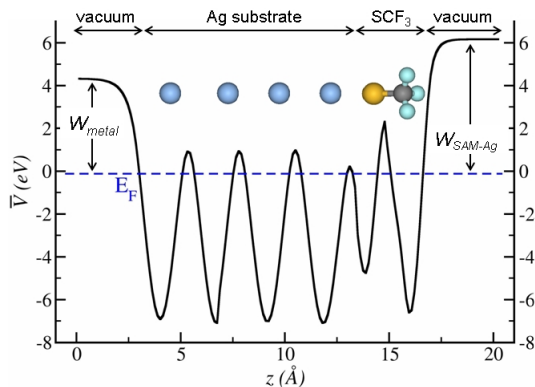


Figure 1. Plane averaged electrostatic potential $\bar{V}(z)$ of a slab consisting of four layers of silver atoms and one layer of CF_3S molecules on top. The z axis is normal to the (111) surface.

functions are evaluated from the expression:

$$W = V(\infty) - E_F, \quad (2)$$

where $V(\infty)$ is the electrostatic potential in vacuum and E_F is the Fermi energy of the bulk metal. $V(\infty)$ is extracted by calculating the average electrostatic potential in the xy -planes of the slab:

$$\bar{V}(z) = \frac{1}{C} \iint_{\text{cell}} V(x, y, z) dx dy, \quad (3)$$

where C is the area of the surface unit cell and $V(x, y, z)$ is the total electrostatic potential. The latter is generated on an equidistant real space grid and the integral is obtained by straightforward numerical integration. In practice $\bar{V}(z)$ reaches an asymptotic value $V(\infty)$ within a distance of $\sim 5\text{\AA}$ from the surface into the vacuum.

An example of $\bar{V}(z)$ is shown in Fig. 1 for CF_3S on the Ag(111) surface. W_{metal} is the work function of the clean Ag surface and $W_{\text{SAM-Ag}}$ is the work function of surface covered by the SAM. Slab calculations produce a reasonable value for the bulk Fermi energy E_F , but a more accurate value is obtained from a separate bulk calculation. We follow the procedure described by Fall *et al.* [32]. From the convergence tests discussed in the previous section we estimate that calculated work functions are converged to within ~ 0.05 eV. Typically, DFT/PW91 calculations give work functions that are within 0.1-0.2 eV of the experimental values, although occasionally larger deviations of ~ 0.3 eV can be found [33, 34].

Upon adsorption of a SAM the work function of a metal surface usually changes considerably. The work function change ΔW can be interpreted in terms of a change in the surface dipole $\Delta\mu$:

$$\Delta W = W_{\text{SAM-metal}} - W_{\text{metal}} = \frac{e\Delta\mu}{\epsilon_0 A}, \quad (4)$$

where A is the surface area per adsorbed molecule [35]. Note that $\Delta\mu$ corresponds to the component of the dipole

moment directed along the surface normal, since only this component affects the work function. $\Delta\mu$ is the result of the interface formation between the SAM and the metal surface, and we call it the *interface dipole* in the following.

We split the interface dipole into a contribution μ_{SAM} from the molecular dipoles in the SAM, and a contribution μ_{chem} from the charge transfer between the metal surface and the molecule, which occurs upon chemisorption of the SAM. The latter contribution is then defined by:

$$\mu_{\text{chem}} = \Delta\mu - \mu_{\text{SAM}}. \quad (5)$$

μ_{SAM} is obtained from a separate calculation on a free-standing SAM without the presence of a metal slab, but with the molecules frozen in their adsorbed geometry. In the following we will show that μ_{chem} is nearly independent of the (fluorinated) alkyl tail of the thiolate molecule. This means that μ_{chem} is mainly determined by the sulfur-metal bond and the charge transfer associated with this bond.

Note that the calculation of μ_{SAM} is done for a full monolayer. In practice μ_{SAM} is obtained from the expression:

$$\mu_{\text{SAM}} = \frac{\epsilon_0 A \Delta V}{e}, \quad (6)$$

where $\Delta V = V(\infty) - V(-\infty)$ is the potential drop over the SAM, and $V(\infty), V(-\infty)$ are the asymptotic electrostatic potentials on both sides of the SAM. These are easily obtained, since the potential reaches its asymptotic values within a distance of few \AA of the SAM.

This calculation incorporates the effect of the depolarizing electric field within the SAM that is generated by the close-packed molecular dipoles. Often this effect is modeled phenomenologically by introducing an effective dielectric constant ϵ for the SAM:

$$\mu_{\text{SAM}} = \frac{\mu_z}{\epsilon}, \quad (7)$$

where μ_z is the z -component of the permanent dipole of the isolated molecule. By obtaining μ_z from a separate calculation we will extract the effective dielectric constant as a function of the packing density of the molecules in the SAM.

3. INFLUENCE OF PACKING DENSITY

We will first discuss the possible structures of thiolate SAMs on the Ag(111) surface and then study the influence of the packing density on the work function.

3.1. Structures

From early scanning tunneling microscopy (STM) experiments it was concluded that SAMs of alkanethiolates on the Ag(111) surface form a commensurate

($\sqrt{7} \times \sqrt{7}$) $R10.9^\circ$ structure [36, 37]. Normal incident X-ray standing wave (NIXSW) experiments have confirmed the $\sqrt{7} \times \sqrt{7}$ structure, but have corrected the registry of the SAM on the underlying substrate to ($\sqrt{7} \times \sqrt{7}$) $R19.1^\circ$ [17]. The proposed model of this structure has the molecules in the SAM arranged in a hexagonal lattice with a nearest neighbor distance between the sulfur atoms of 4.41 Å, see Fig. 2(a). Long chain alkanethiolates adopt an expanded incommensurate ($\sqrt{7} \times \sqrt{7}$) $R19.1^\circ$ structure with a nearest neighbor distance of 4.6-4.8 Å [38, 39], whereas short chain alkanethiolates keep the commensurate structure [17]. Recently a new model has been proposed for the ($\sqrt{7} \times \sqrt{7}$) $R19.1^\circ$ structure of CH_3S SAMs on Ag(111) on the basis of NIXSW and medium energy ion scattering (MEIS) experiments [18, 40, 41]. It involves a surface reconstruction consisting of a $3/7$ monolayer of Ag adatoms, which are bonded to the methylthiolate molecules, Fig. 2(c).

The ($\sqrt{7} \times \sqrt{7}$) $R19.1^\circ$ structure proposed first consists of three molecules per surface unit cell with two of the molecules adsorbed on hollow sites and one on a top site [17]. Starting from this structure we have relaxed the geometry of CH_3S on Ag(111) and the result is shown in Fig. 2(a) and (b). The molecules labeled 1 and 3 change their position only slightly and remain adsorbed in a hollow site. The molecule labeled 2 moves away from the top site towards a bridge site. The angle between the surface normal and the C–S bond is 42° , whereas that angle for molecules 1 and 3 is only $9\text{--}10^\circ$. The latter molecules are almost standing upright, as can be observed in Fig. 2(b). We call this structure the “1,3 hollow” structure in the following. The most important bond distances and angles of this structure are given in Table I. The adsorption energy (averaged, per molecule) according to Eq. (1) is -1.97 eV.

In our previous calculations for alkanethiolate SAMs on Au(111) the molecules show a strong preference for adsorption on bridge sites, instead of on hollow or top sites [15]. Starting with CH_3S molecules 1 and 3 on bridge positions we obtain the optimized geometry that is shown in Figs. 2(e) and (f). In this structure the CH_3S molecule 2 also moves closer to the bridge position, as compared to the 1,3 hollow structure, see Table I. The new structure, which we call the “bridge” structure, is 0.10 eV/molecule lower in energy than the 1,3 hollow structure. The bridge structure is energetically favored over the 1,3 hollow structure. The calculated adsorption energy in the bridge structure is -2.07 eV/molecule. The geometries of the three molecules in the bridge structure are more similar than in the 1,3 hollow structure. For instance, the angle between the surface normal and the C–S bond is in the range $43\text{--}51^\circ$ for all three molecules, see Table I. The work functions of the 1,3 hollow and the bridge structures are substantially different as will be discussed below.

We have also optimized the geometry in the ($\sqrt{7} \times \sqrt{7}$) $R19.1^\circ$ reconstructed structure [18, 41]. The

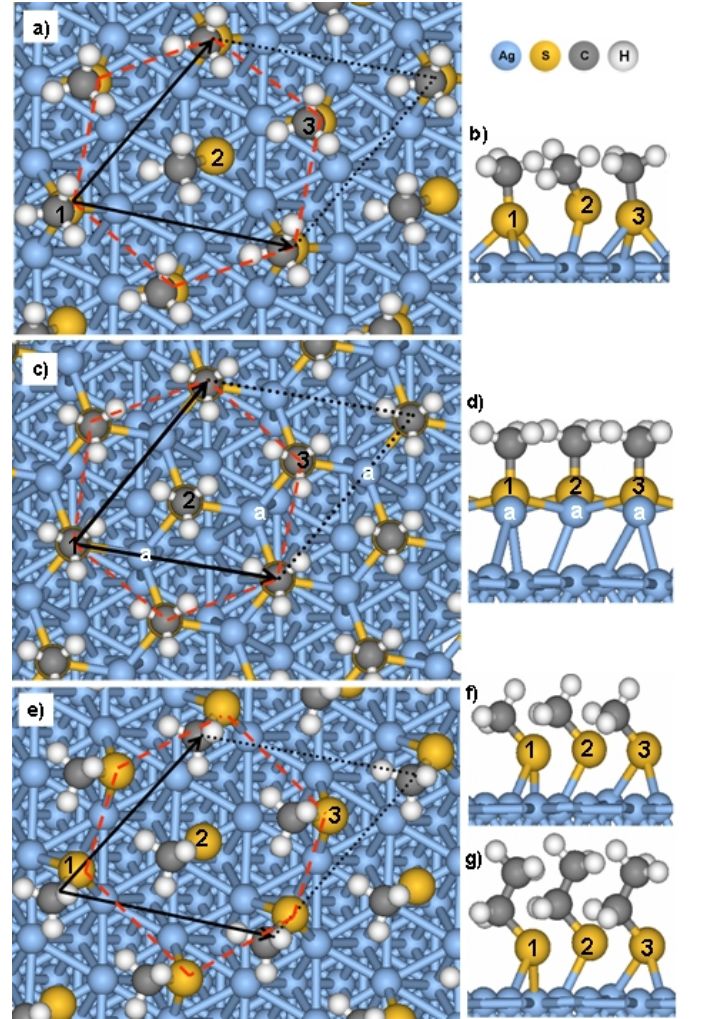


Figure 2. Possible ($\sqrt{7} \times \sqrt{7}$) $R19.1^\circ$ structures of CH_3S SAMs on Ag(111); (a), (b) top and side view of the 1,3 hollow structure; (c), (d) of the reconstructed structure; (e), (f) of the bridge structure; (g) of a $\text{C}_2\text{H}_5\text{S}$ SAM in the bridge structure. “1, 2, 3” label the molecules, “a” labels the Ag adatoms.

reconstruction involves a commensurate layer of Ag adatoms at a $3/7$ monolayer coverage. The sulfur atoms of the adsorbed thiolate molecules are threefold coordinated by adatoms. The optimized geometry is shown in Figs. 2(c) and (d) and bond distances and angles of this structure are given in Table I. The resulting structure has the CH_3S molecules standing upright with the C–S bond pointing along the surface normal in agreement with previous calculations [28, 42]. The distance of the S atoms of the different molecules to the surface is the same within ~ 0.1 Å, which represents a very small “rumpling” in agreement with the latest experimental results [41]. The work function of the reconstructed structure is substantially different from that of the unreconstructed structures as will be discussed below. The calculated adsorption energy in the reconstructed structure is -2.07

	1,3 hollow		
	molecule 1	2	3
C-H(Å)	1.10	1.10	1.10
S-C(Å)	1.83	1.84	1.84
Ag-S(Å)	2.52/2.50/2.50	2.47/3.01	2.63/2.54/2.54
C-S-normal(°)	9.0	42.0	9.7
Ag-S-Ag(°)	78.7/77.5/77.4	-	76.2/71.3/72.5
	bridge		
	molecule 1	2	3
C-H(Å)	1.10	1.10	1.10
S-C(Å)	1.83	1.84	1.83
Ag-S(Å)	2.56/2.49	2.46/2.82	2.58/2.48
C-S-normal(°)	51.4	43.0	46.6
Ag-S-Ag(°)	72.3	-	72.5
	reconstructed		
	molecule 1	2	3
C-H(Å)	1.10	1.10	1.10
S-C(Å)	1.84	1.84	1.84
Ag-S(Å)	2.65	2.66	2.64
C-S-normal(°)	0	0	0
Ag-S-Ag(°)	114.9	115.3	115.9
d_z	2.47	2.56	2.47

TABLE I: Bond lengths and bond angles of the $(\sqrt{7} \times \sqrt{7})R19.1^\circ$ 1,3 hollow, bridge and reconstructed structures of CH_3S SAMs on Ag(111). The columns indicate the three molecules in the supercell, see Fig. 2. d_z is the distance along the surface normal between a Ag adatom and the top Ag layer.

eV/molecule. This number is very close to the adsorption energy in the (unreconstructed) bridge structure. Within the intrinsic error bar of DFT calculations the two structures are degenerate in energy. It has recently been suggested that the two structures, i.e. reconstructed and unreconstructed, might coexist on the surface [42].

The optimized unreconstructed $(\sqrt{7} \times \sqrt{7})R19.1^\circ$ structure of a $\text{CH}_3\text{CH}_2\text{S}$ SAM also has the molecules adsorbed on or near bridge sites, as shown in Fig. 2(g). The three molecules in the unit cell have a similar geometry. For instance, the C-S-normal angle is 42-45°, see Table II, which is similar to the experimental value reported for $\text{CH}_3(\text{CH}_2)_7\text{S}$ on Ag(111) [17]. The chain angles are in the range 12-17°, which is similar to experimental results for long-chain alkanethiolates [43].

We have also studied $(\sqrt{3} \times \sqrt{3})R30^\circ$ and $p(2 \times 2)$ structures, where the surface area per adsorbed molecule is 29% and 71% larger, respectively, see Fig. 3. Experimentally it is not likely that alkanethiolates on Ag(111) form these structures, but they enable us to model the influence of the packing density of the molecules in the SAM on the work function and the interface dipoles. In both these structure the bridge site is the favored adsorption site and the local geometry of the molecules is similar to that in the $(\sqrt{7} \times \sqrt{7})R19.1^\circ$ bridge structure.

The structure of (partially) fluorinated alkanethiolates is much less established than that of their nonfluorinated counterparts. On Au(111) thiols with long fluorinated alkyl tails have a less dense packing because of their relatively bulky tails [9, 44]. For such SAMs a $p(2 \times 2)$ struc-

	molecule 1	2	3
C-H(Å)	1.10	1.10	1.10
C-C(Å)	1.52	1.53	1.52
S-C(Å)	1.85	1.85	1.84
Ag-S(Å)	2.57/2.50	2.47/2.90	2.58/2.49
C-C-normal(°)	25.5	26.3	26.8
C-S-normal(°)	44.2	41.9	45.0
chain(°)	14.7	12.0	17.1
Ag-S-Ag(°)	72.1	-	72.5

TABLE II: Bond lengths and bond angles of the $(\sqrt{7} \times \sqrt{7})R19.1^\circ$ bridge structure of $\text{CH}_3\text{CH}_2\text{S}$ SAMs on Ag(111). The chain angle represents the angle made by the line connecting the top C and S atoms with the surface normal.

ture has been proposed, where the spacing between the adsorbate molecules is 5.87 Å [45]. SAMs of long-chain alkanethiolates with fluorinated end groups on Au(111) have a $(\sqrt{3} \times \sqrt{3})R30^\circ$ structure [46]. The spacing between the adsorbate molecules is then 5.08 Å.

We did not find reports on the structural details of fluorinated alkanethiolate SAMs on silver in the literature. We optimized the structure of CF_3S and $\text{CF}_3\text{CH}_2\text{S}$ SAMs on Ag(111) in three different packing densities, i.e., $(\sqrt{7} \times \sqrt{7})$, $(\sqrt{3} \times \sqrt{3})$ and $p(2 \times 2)$. For the $(\sqrt{7} \times \sqrt{7})R19.1^\circ$ structure of a CF_3S SAM, which represents the most dense packing, we used the 1,3 hollow and the bridge structures of CH_3S as starting points and optimized the geometry. The bridge structure of CF_3S is more stable than the 1,3 hollow structure, albeit by less than 0.02 eV/molecule. However, even in the bridge structure only molecules 1 and 3 are actually adsorbed on bridge sites, whereas molecule 2 is adsorbed on a hollow site. This results in a distorted hexagonal packing of the CF_3S molecules.

For the $(\sqrt{3} \times \sqrt{3})R30^\circ$ and $p(2 \times 2)$ structures of fluorinated alkanethiolate SAMs on Au(111) we have found a preference for the molecules to adsorb on bridge sites [15]. The calculated nearest neighbor distance between the metal atoms on Au(111) and Ag(111) is very similar, i.e., 2.94 and 2.93 Å respectively. Moreover, since even in the $(\sqrt{7} \times \sqrt{7})$ structure the molecules show a tendency to adsorb on bridge sites, we only consider bridge sites for the $(\sqrt{3} \times \sqrt{3})$ and $p(2 \times 2)$ structures of SAMs on Ag, see Fig. 3.

Table III lists the molecular geometries of CF_3S and $\text{CF}_3\text{CH}_2\text{S}$ SAMs on Ag(111) adsorbed in bridge structures for the different packings. The geometries are in fact very similar, with S-Au bond lengths in the range 2.5-2.6 Å, and angles of the C-S bond with the surface normal around 45°. In the case of $\text{CF}_3\text{CH}_2\text{S}$ the chain angle is 13-15°, which is similar to that found in $\text{CH}_3\text{CH}_2\text{S}$, see Table I.

The calculated adsorption energies indicate that a less dense packing of the fluorinated alkanethiolate SAMs is favorable, see Table III. The $p(2 \times 2)$ structure is most sta-

	CF ₃ S		
	$\sqrt{7} \times \sqrt{7}$	$\sqrt{3} \times \sqrt{3}$	$p(2 \times 2)$
C-F(Å)	1.35/1.36/1.35	1.36	1.36
S-C(Å)	1.85/1.83/1.87	1.84	1.84
Ag-S(Å)	2.51/2.41/2.57	2.56	2.54
C-S-normal(°)	6.5/35.5/5.0	43.2	47.7
Ag-S-Ag(°)	79/-/72	73.4	71.5
E_{ads} (eV)	-1.98	-2.32	-2.39
	CF ₃ CH ₂ S		
	$\sqrt{7} \times \sqrt{7}$	$\sqrt{3} \times \sqrt{3}$	$p(2 \times 2)$
C-F(Å)	1.35	1.36	1.36
C-C(Å)	1.52	1.52	1.52
C-H(Å)	1.10	1.09	1.09
S-C(Å)	1.84	1.85	1.85
Ag-S(Å)	2.53/2.45/2.52	2.56	2.56
C-C-normal(°)	25.9/25.7/29.0	25.8	21.0
C-S-normal(°)	44.0/42.4/42.7	42.8	46.7
chain(°)	13.9/12.9/15.1	12.3	16.7
Ag-S-Ag(°)	72.5/-/73.5	72.1	72.0
E_{ads} (eV)	-2.01	-2.27	-2.24

TABLE III: Bond lengths, bond angles and adsorption energies of CF₃S and CF₃CH₂S SAMs adsorbed on Ag(111) surface in $(\sqrt{7} \times \sqrt{7})R19.1^\circ$, $(\sqrt{3} \times \sqrt{3})R30^\circ$ and $p(2 \times 2)$ structures. The chain angle represents the angle made in the CF₃CH₂S SAM by the top C atom and the sulfur atom with the surface normal.

ble for CF₃S, whereas for CF₃CH₂S the $(\sqrt{3} \times \sqrt{3})R30^\circ$ is slightly more stable. Some of the energy differences are quite small, but the calculations correspond to the experimental trend observed in fluorinated alkanethiolates on Au(111) [45, 46].

3.2. Work functions and interface dipoles

The change in work function upon adsorption of a SAM is defined by Eq. (4). For the clean Ag(111) surface we calculate a work function of 4.50 eV, using a 25×25 **k**-point Brillouin zone sampling grid. This is in good agreement with the experimental results of 4.5 eV [47] and 4.4 eV [7], and with a previously reported theoretical value of 4.42 eV, which was extracted from DFT-GGA calculations and a 15×15 **k**-point sampling [48]. The calculated work function changes upon adsorption of the (fluorinated) alkanethiolate SAMs are given in Table IV.

The results clearly show that alkanethiolates decrease the work function, whereas fluorinated alkanethiolates increase it significantly. Depending on the structure, a difference of 2-2.5 eV is found between the work functions of alkanethiolates and partially fluorinated alkanethiolates adsorbed on the silver surface. The work function is thus tunable over a large range by adsorption of a suitable SAM, as is observed experimentally [5, 7]. The absolute change in the work function upon adsorption of fluorinated alkanethiolates is 3-4 times larger than the change upon adsorption of nonfluorinated molecules. This result is quite different from our previous findings for SAMs on

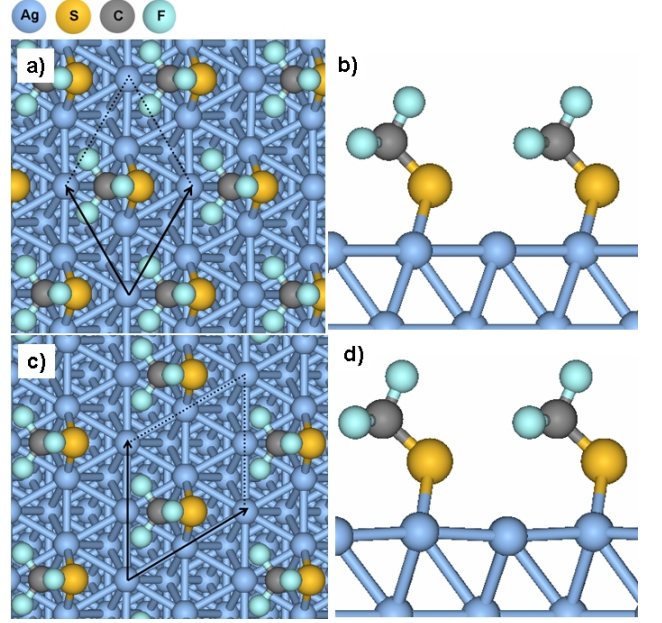


Figure 3. CF₃S SAM on Ag(111) with the molecules adsorbed on bridge sites; (a),(b) top and side view of the $(\sqrt{7} \times \sqrt{7})R19.1^\circ$ structure; (c),(d) of the $p(2 \times 2)$ structure.

Au(111), where fluorinated and nonfluorinated molecules give a change in the work function that is similar in size (but of opposite sign, of course) [15]. We conclude that the interaction between the molecules and the silver surface differs from that between the molecules and the gold surface.

Kelvin probe measurements of the work function changes induced by adsorption of long-chain thiolate SAMs on Ag(111) have been reported by Campbell *et al.* [5], and by de Boer *et al.* [7]. The values reported for CH₃(CH₂)₉S and CH₃(CH₂)₁₅S are -0.7 eV [5], and -0.6 eV [7], respectively, and 0.9 eV [5] and 1.1 eV [7] for CF₃(CF₂)₇(CH₂)₂S. Our calculated value of -0.59 eV for CH₃CH₂S in the $(\sqrt{7} \times \sqrt{7})R19.1^\circ$ bridge structure is close to the experimental values for alkanethiolates. The calculated values for the fluorinated molecules are higher than the experimental values even for the less densely packed $p(2 \times 2)$ structure. One explanation might be that the effective dipole moment of a long-chain fluorinated molecule embedded in a SAM is smaller than that of a short-chain molecule; in other words, the effective dielectric constant in a long-chain fluorinated thiolate SAM is larger, see Eq. (7). In addition, SAMs of fluorinated alkanethiolates may show more intrinsic disorder than their nonfluorinated counterparts [46], which also reduces the average dipole moment perpendicular to the surface.

The three $\sqrt{7} \times \sqrt{7}$ structures for CH₃S SAMs discussed in the previous section give rise to different work functions. The adsorption of molecules in the bridge structure gives a substantial smaller shift of the work function than adsorption in the 1,3 hollow structure or

	$\sqrt{7} \times \sqrt{7}$	$\sqrt{3} \times \sqrt{3}$	p(2×2)
CH ₃ S	-0.52 (-0.84 ^a , -0.99 ^b)	-0.61	-0.34
CH ₃ CH ₂ S	-0.59	-0.52	-0.46
CF ₃ S	1.80 (1.79 ^a)	1.61	1.48
CF ₃ CH ₂ S	2.09	1.75	1.75

TABLE IV: Work functions shifts in eV with respect to the clean surface of SAMs on Ag(111) in the bridge structure; ^{a,b} in the 1,3 hollow and the reconstructed structure, respectively.

the reconstructed structure. Using Eq. (4) we can interpret the changes in the work function in terms of molecular dipoles. This difference in work function shift between the structures can be related to the orientation of the molecular dipoles. Whereas in the bridge structure the molecular tails are tilted with respect to the surface normal, the tails of the two molecules that are adsorbed at hollow sites in the 1,3 hollow structure are almost perpendicular to the surface, see Table I. The latter leads to larger dipole moments along the surface normal. All the molecular tails in the reconstructed structure are perpendicular to the surface, which leads to large dipole moments and a large work function shift. These results suggest that work function measurements might be a simple experimental way of distinguishing between the different structures.

As can be observed in Table IV, the work functions have a relatively weak dependence on the packing density. The local geometries of the thiolate molecules in the bridge structure are similar for the different packings, see e.g. Table III. Hence one would expect the individual molecular dipoles to be similar. The weak dependence of the work functions on the packing density might seem somewhat surprising. Assuming fixed interface dipoles $\Delta\mu$ per molecule in Eq. (4), the work functions should scale as $1/A$, where A is the surface area per molecule. Since this is clearly not the case, it means that $\Delta\mu$ depends on the packing density. In particular, the individual molecular dipoles increase with decreasing packing density.

Decreasing the packing density increases the distances between the molecules in the SAM. Hence it decreases the depolarizing field in the SAMs, or, in other words, the effective dielectric constant ε introduced in Eq. (7) decreases with decreasing packing density. This effectively increases the molecular dipoles, which opposes the effect of a decreasing density of the molecules on the interface dipole. The net result is a weak dependence of the work function on the packing density in the range considered and in some cases even a nonmonotonic behavior, see Table IV.

In order to quantify this analysis we make use of the relations given by Eqs. (4)-(7). We extract from the work function change an interface dipole per molecule $\Delta\mu$ and split $\Delta\mu$ into a contribution μ_{SAM} from the molecular dipole and a contribution μ_{chem} from the charge transfer

between the molecule and the surface upon chemisorption. The results for each of the SAMs in the $\sqrt{7} \times \sqrt{7}$, $\sqrt{3} \times \sqrt{3}$ and p(2×2) structures are reported in Table V. As we are explicitly interested in the influence of the packing density we continue to compare similar, i.e. bridge-like, structures.

μ_{SAM} is positive for fluorinated alkanethiolates, which means that the molecular dipoles point from the S atom to the CF₃ group. For the nonfluorinated alkanethiolates the absolute values of μ_{SAM} are larger, but the sign is negative, meaning that the dipoles point from the alkyl tails to the S atom. μ_{chem} is positive for all molecules. The latter contribution is associated with a dipole that points from the surface to the molecule. It is associated with a (partial) electron transfer from the surface to the molecule. Both contributions, μ_{SAM} and μ_{chem} , to the interface dipole $\Delta\mu$ are of comparable size. For the nonfluorinated molecules they are of opposite sign, which leads to moderate interface dipoles $\Delta\mu = -0.2$ to -0.3 D and work function changes $\lesssim 0.5$ eV. The contributions μ_{SAM} and μ_{chem} have the same sign for the fluorinated molecules, which gives large interface dipoles $\Delta\mu = 0.9$ -1.3 D and large work function changes of up to 2-2.5 eV.

Comparing the results for the different packing densities in Table V, we observe that the absolute value of μ_{SAM} increases if the packing density decreases. This can be understood by noting that the effective dielectric constant ε of the SAM decreases if the packing density decreases, as discussed above. We have calculated the dipole moment of the isolated alkanethiolate radical molecules, fixing the molecules in the geometries they attain in the SAM. The component μ_z along the surface normal in the adsorbed geometry is given in Table VI. From Eq. (7) we then calculate the effective dielectric constant of the free standing SAM. The dielectric constants for fluorinated alkanethiolate SAMs are somewhat larger than those of their nonfluorinated counterparts. This might be expected since the polarizability of fluorinated molecules is larger and therefore screening in the SAM is larger. The results in Table V clearly show that the dielectric constants decrease with decreasing packing density.

μ_{chem} also increases with decreasing packing density. The origin of this effect is similar to that discussed in the previous paragraph; the screening of the dipoles in the layer decreases if the packing density decreases. An interesting observation is that at fixed packing density μ_{chem} shows little variation within the range of molecules. Apparently it is mainly determined by the S-Ag interaction and not so much by the molecular tails.

Upon adsorption electronic charge is transferred from the surface to the molecule. In order to visualize the charge transfer at the interface upon adsorption of the SAMs, we calculate the change in electron density Δn :

$$\Delta n = n_{\text{SAM-Ag}} - n_{\text{Ag}} - n_{\text{SAM}}, \quad (8)$$

where $n_{\text{SAM-Ag}}$, n_{Ag} and n_{SAM} are the electron densities

	$\sqrt{7} \times \sqrt{7}$				$\sqrt{3} \times \sqrt{3}$				p(2×2)			
	CH ₃ S	C ₂ H ₅ S	CF ₃ S	CF ₃ CH ₂ S	CH ₃ S	C ₂ H ₅ S	CF ₃ S	CF ₃ CH ₂ S	CH ₃ S	C ₂ H ₅ S	CF ₃ S	CF ₃ CH ₂ S
$\Delta\mu$	-0.24	-0.27	0.83	0.96	-0.36	-0.31	0.95	1.04	-0.27	-0.36	1.17	1.38
μ_{SAM}	-0.78	-0.79	0.39	0.43	-0.88	-0.79	0.44	0.50	-0.92	-1.01	0.50	0.71
μ_{chem}	0.54	0.52	0.44	0.53	0.52	0.46	0.51	0.54	0.65	0.65	0.67	0.67
ε	1.6	1.4	2.0	2.7	1.4	1.4	1.8	2.3	1.3	1.1	1.6	1.7

TABLE V: Dipole per molecule $\Delta\mu$ from work function shift upon adsorption, the (perpendicular) molecular dipole moment μ_{SAM} in a free standing SAM and the chemisorption dipole moment μ_{chem} of the SAMs on Ag(111) surface. The values are in D. ε is the effective dielectric constant of the free standing SAM.

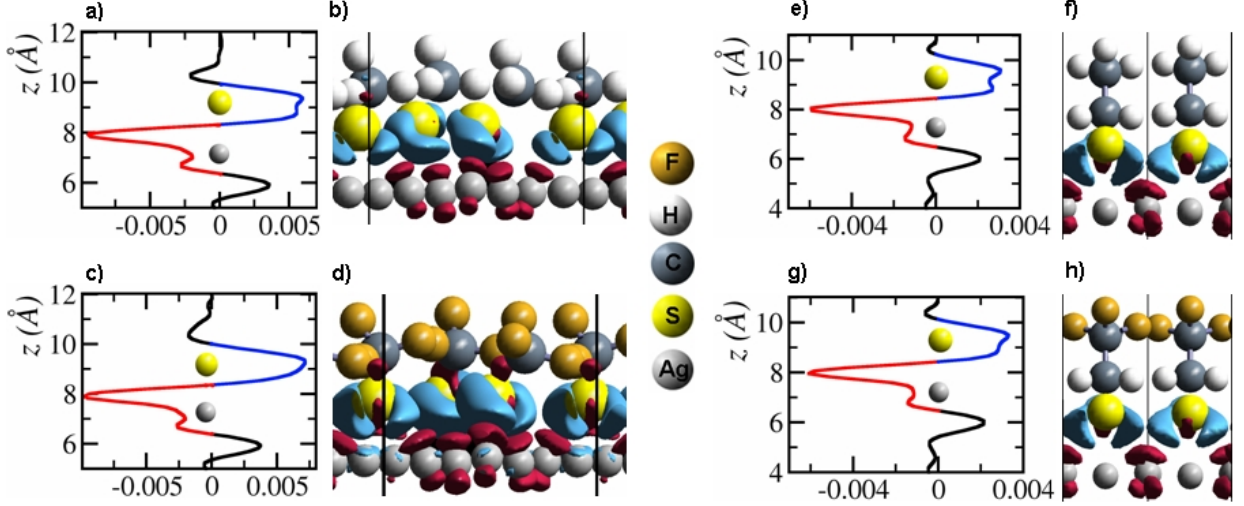


Figure 4. Difference electron density along the surface normal (z) averaged over the xy plane in units of \AA^{-3} and as isodensity surface. (a), (b) CH₃S and (c), (d) and CF₃S in the $\sqrt{7} \times \sqrt{7}$ structure; (e), (f) CH₃CH₂S and (g), (h) CF₃CH₂S in the p(2×2) structure.

of the SAM adsorbed on Ag(111), of the Ag(111) surface and of the free-standing SAM, respectively. The electron distributions are obtained on a real space grid from separate calculations on the adsorbed SAM, on the substrate and on the free-standing SAM, respectively. In the latter two calculations the substrate and the molecules are fixed in the adsorption geometries.

As examples, Fig. 4 shows the difference electron density Δn averaged in the xy plane along the surface normal of CH₃S and CF₃S SAMs adsorbed in the $\sqrt{7} \times \sqrt{7}$ structure and of CH₃CH₂S and CF₃CH₂S SAMs adsorbed in the p(2×2) structure. In addition three dimensional visualizations of Δn at the interface are presented. Only the region around the SAM/Ag(111) interface is shown, since in the substrate and the vacuum region $\Delta n \simeq 0$. The figures clearly demonstrate that Δn is localized at the interface, i.e., near the sulfur atoms and the top metal layer. Electronic density is transferred mainly from the top layer of silver atoms to the sulfur atoms, which results in a dipole moment μ_{chem} .

To check the consistency of this analysis, we can calculate the metal-sulfur dipoles from the difference electron

density:

$$\mu'_{\text{chem}} = \int \int \int_{z_o}^{z_v} z \Delta n(x, y, z) dx dy dz, \quad (9)$$

where we choose z_o in the center between the second and the third metal layer of the substrate and z_v in the center of the vacuum. The metal-sulfur dipoles μ'_{chem} are within 10% of the values μ_{chem} listed in Table V.

By integrating the peak of Δn on the sulfur atom, see Fig. 4, one can calculate the charge transfer from the substrate to the sulfur atom. A typical value over a range of structures is $q = (0.11 \pm 0.01)e$. Modeling the charge transfer dipole as $\mu_{\text{chem}} = qd$ gives $d = 1.1 \text{\AA}$, assuming $\mu_{\text{chem}} = 0.6 \text{ D}$. The distance between the sulfur atoms and the top layer of silver atoms is 2.0-2.2 \AA , so this analysis is consistent with the interpretation of μ_{chem} as a metal-sulfur bond dipole.

The fact that this dipole moment hardly depends on the different molecular tails is slightly surprising, since the electronegativity of fluorinated tails is much higher than that of unfluorinated ones. The Mulliken electronegativity of a molecule is defined as:

$$\chi_M = \frac{EA + IP}{2}, \quad (10)$$

	CH ₃ S	C ₂ H ₅ S	CF ₃ S	CF ₃ CH ₂ S
<i>EA</i>	1.73	1.87	3.02	2.43
<i>IP</i>	9.20	8.95	10.79	9.82
χ_M	5.47	5.41	6.91	6.13
$ \mu_{\text{tot}} $	1.70	1.82	1.05	2.06
μ_z	-1.23	-1.14	0.79	1.17

TABLE VI: Electron affinity (EA), ionization potential (IP), Mulliken electronegativity (χ_M) in eV, total dipole moment $|\mu_{\text{tot}}|$ and dipole moment along the surface normal μ_z in D of isolated molecules in their adsorbed geometries.

where *EA* and *IP* are the electron affinity and ionization potential of the molecule. The *EAs*, *IPs* and Mulliken electronegativities of the molecules considered in this paper (fixed in their adsorbed geometries) are given in Table VI.

One observes a considerable difference in the electronegativities χ_M of the molecules. The χ_M of both alkanethiolates is similar, but the χ_M of fluorinated alkanethiolates is much larger. The HOMO of the radical neutral molecules, which plays a role in determining the *EA* and *IP*, is stabilized by the electron withdrawing CF₃ group. This property is commonly associated with the attractive Coulomb field of the CF₃ group. The HOMO of the neutral molecules is localized mainly on the sulfur atom and one expects that the effect of the CF₃ group decreases if the distance between this group and the sulfur atom increases. Indeed one finds that the *EA*, *IP* and χ_M of CF₃S are significantly higher than those of CF₃CH₂S.

The electronegativity of a metal surface is given by its work function. From simple chemical reasoning one would assume that the charge transfer between a molecule and a surface would depend on the difference of their electronegativities. This is clearly not the case; the electronegativity of the molecule does not seem to influence the charge transfer. This suggests that the effects of the Coulomb field of the CF₃ group and the alkyl tails on the charge distribution at the sulfur-metal interface are screened by the metal.

4. SUMMARY AND CONCLUSIONS

We have studied the interface dipole formation and work function changes produced by adsorption of CH₃S, CH₃CH₂S, CF₃S and CF₃CH₂S SAMs on the Ag(111) surface by means of DFT calculations. Adsorption of the alkanethiolates CH₃S and CH₃CH₂S decreases the work function as compared to the clean metal surface, whereas adsorption of the fluorinated alkanethiolates CF₃S and CF₃CH₂S increases the work function.

In particular we have examined the influence of the structure and the packing density of the molecules in the SAM. CH₃S on Ag(111) in the unreconstructed ($\sqrt{7} \times \sqrt{7}$)R19.1° structure with two of the three

molecules in the unit cell adsorbed at a hollow site, leads to a work function shift of -0.8 eV. Adsorbing the CH₃S molecules on bridge sites stabilizes the structure by 0.10 eV/molecule and gives a work function shift of -0.5 eV. The recently proposed surface reconstruction induced by CH₃S adsorption yields an almost identical adsorption energy, and a work function shift of -1.0 eV. The difference between the work functions of these structures can be interpreted in terms of the difference in the orientation of the molecular dipoles.

These results are compared to the less densely packed ($\sqrt{3} \times \sqrt{3}$)R30° and p(2×2) structures, which are more likely to occur for fluorinated alkanethiolate SAMs. Although the work function shift generally decreases for decreasing packing density, it is not simply proportional to the density of molecular dipoles. A partial compensating effect is caused by a decrease of the dielectric screening in the molecular layer.

Comparing the different molecules adsorbed in similar geometries shows that fluorinated alkanethiolates can increase the work function by up to 2 eV, which is much larger than the decrease in work function caused by (non-fluorinated) alkanethiolate adsorption. We explain this by separating the interface dipole into a contribution from the molecular dipoles and from the charge reordering at the metal-SAM interface. Electron transfer occurs from the Ag surface to the sulfur atoms of the thiolate molecules. The resulting dipole points in the same direction as the molecular dipole for fluorinated molecules. Addition of the two dipoles leads to a large interface dipole and a large work function shift. The direction of the molecular dipole of nonfluorinated molecules is opposite to the metal-sulfur bond dipole, resulting in a much smaller interface dipole and work function shift.

The electron transfer from the Ag surface to the molecules is remarkably independent of the electronegativity of the molecules. In good approximation the charge reordering only depends upon the metal-sulfur bond, which suggests that the influence of the molecular tails is screened by the metal substrate. In previous calculations we arrived at the same conclusion for adsorption of alkanethiolate SAMs on other noble metal surfaces, indicating that this result is more general [15, 16]. For adsorption on Ag(111) we find effective Ag-S dipoles $\mu_{\text{chem}} = 0.51 \pm 0.04$ D and 0.66 ± 0.01 D in the ($\sqrt{3} \times \sqrt{3}$) and p(2×2) structures, respectively.

For adsorption on Au(111) we have found very small Au-S dipoles $\mu_{\text{chem}} < 0.1$ D, indicating an apolar Au-S bond [15], whereas for adsorption on Pt(111) the Pt-S dipole is $\mu_{\text{chem}} = -0.45 \pm 0.03$ D [16]. The latter indicates an electron transfer from the sulfur atoms to the Pt surface. The metal-sulfur bonds formed upon SAM adsorption generate dipole moments that reduce the work function differences between the clean metal surfaces, and can even reverse the order. The molecular dipole moments exhibit similar values for adsorption on Ag, Au and Pt, thus giving the possibility to design interface dipoles. By adding molecular and metal-sulfur bond dipoles the over-

all work function can be determined. It is possible to manipulate metal work functions considerably using SAMs. Work function shifts that can be as large as 2 eV.

Acknowledgments

This work is supported by “Prioriteits Programma Materialenonderzoek” (PPM), by the “Stichting voor Fundamenteel Onderzoek der Materie” (FOM), financially supported by the “Nederlandse Organisatie voor Wetenschappelijk Onderzoek” (NWO), and by “NanoNed”, a nanotechnology program of the Dutch Ministry of Economic Affairs. The use of supercomputer facilities was sponsored by the “Stichting Nationale Computer Faciliteiten” (NCF), financially supported by NWO.

References and Notes

- [1] Lee, J. K.; Lee, K.-B.; Kim, D. J.; Choi, I. S. *Langmuir* **2003**, *19*, 8141–8143.
- [2] Swalen, J. D.; Allara, D. L.; Andrade, J. D.; Chandross, E. A.; Garoff, S.; Israelachvili, J.; McCarthy, T. J.; Murray, R.; Pease, R. F.; Rabolt, J. F.; Wynne, K. J.; Yu, H. *Langmuir* **1987**, *3*, 932–950.
- [3] Chen, C. S.; Mrksich, M.; Huang, S.; Whitesides, G. M.; Ingber, D. E. *Biotechnol. Prog.* **1998**, *14*, 356–363.
- [4] Parker, I. D. *J. Appl. Phys* **1994**, *75*, 1656–1666.
- [5] Campbell, I. H.; Rubin, S.; Zawodzinski, T. A.; Kress, J. D.; Martin, R. L.; Smith, D. L.; Barashkov, N. N.; Ferraris, J. P. *Phys. Rev. B* **1996**, *54*, 14321–14324.
- [6] Campbell, I. H.; Kress, J. D.; Martin, R. L.; Smith, D. L.; Barashkov, N. N.; Ferraris, J. P. *Appl. Phys. Lett.* **1997**, *71*, 3528–3530.
- [7] de Boer, B.; Hadipour, A.; Mandoc, M. M.; van Woudenberg, T.; Blom, P. W. M. *Adv. Mater.* **2005**, *17*, 621–625.
- [8] Poirier, G. E. *Langmuir* **1999**, *15*, 1167–1175.
- [9] Schreiber, F. *Prog. Surf. Sci.* **2000**, *65*, 151–256.
- [10] Vargas, M. C.; Giannozzi, P.; Selloni, A.; Scoles, G. *J. Phys. Chem. B* **2001**, *105*, 9500.
- [11] Morikawa, Y.; Hayashi, T.; Liew, C. C.; Nozoye, H. *Surf. Sci.* **2002**, *507*, 46–50.
- [12] Renzi, V. D.; Rousseau, R.; Marchetto, D.; Biagi, R.; Scandolo, S.; del Pennino, U. *Phys. Rev. Lett.* **2005**, *95*, 046804.
- [13] Heimel, G.; Romaner, L.; Brédas, J.-L.; Zojer, E. *Phys. Rev. Lett.* **2006**, *96*, 196806.
- [14] Rousseau, R.; Renzi, V. D.; Mazzarello, R.; Marchetto, D.; Biagi, R.; Scandolo, S.; del Pennino, U. *J. Phys. Chem. B* **2006**, *110*, 10862–10872.
- [15] Rusu, P. C.; Brocks, G. *J. Phys. Chem. B* **2006**, *110*, 22628–22634.
- [16] Rusu, P. C.; Brocks, G. *Phys. Rev. B* **2006**, *74*, 073414.
- [17] Rieley, H.; Kendall, G. K.; Jones, R. G.; Woodruff, D. P. *Langmuir* **1999**, *15*, 8856–8866.
- [18] Yu, M.; Woodruff, D. P.; Bovet, N.; Satterly, C. J.; Lovelock, K.; Jones, R. G.; Dhanak, V. *J. Phys. Chem. B* **2006**, *110*, 2164.
- [19] Neugebauer, J.; Scheffler, M. *Phys. Rev. B* **1992**, *46*, 16067–16080.
- [20] Hohenberg, P.; Kohn, W. *Phys. Rev.* **1964**, *136*, B864–B871.
- [21] Perdew, J. P.; Chevary, J. A.; Vosko, S. H.; Jackson, K. A.; Pederson, M. R.; Singh, D. J.; Fiolhais, C. *Phys. Rev. B* **1992**, *46*, 6671–6687.
- [22] Kresse, G.; Hafner, J. *Phys. Rev. B* **1993**, *47*, (R)558.
- [23] Kresse, G.; Furthmüller, J. *Phys. Rev. B* **1996**, *54*, 11169.
- [24] Kresse, G.; Joubert, D. *Phys. Rev. B* **1999**, *59*, 1758.
- [25] Blöchl, P. E. *Phys. Rev. B* **1994**, *50*, 17953.
- [26] Methfessel, M.; Paxton, A. T. *Phys. Rev. B* **1989**, *40*, 3616–3621.
- [27] Blöchl, P. E.; Jepsen, O.; Andersen, O. K. *Phys. Rev. B* **1994**, *49*, 16223.
- [28] He, G.-M. *Phys. Rev. B* **2006**, *74*, 245421.
- [29] M.W.Schmidt.; K.K.Baldrige.; J.A.Boatz.; S.T.Elbert.; M.S.Gordon.; J.J.Jensen.; S.Koseki.; N.Matsunaga.; K.A.Nguyen.; S.Su.; T.L.Windus.; M.Dupuis.; J.A.Montgomery. *J. Comput. Chem.* **1993**, *14*, 1347–1363.
- [30] Becke, A. D. *J. Chem. Phys.* **1993**, *98*, 5642–5648.
- [31] P.J.Stephens.; F.J.Devlin.; C.F.Chabrowski.; M.J.Frisch. *J. Phys. Chem.* **1994**, *98*, 11623–11627.
- [32] Fall, C. J.; Binggeli, N.; Baldereschi, A. *J. Phys.: Condens. Matter* **1999**, *11*, 2689–2696.
- [33] Michaelides, A.; Hu, P.; Lee, M.-H.; Alavi, A.; King, D. A. *Phys. Rev. Lett.* **2003**, *90*, 246103.
- [34] Favot, F.; Corso, A. D.; Baldereschi, A. *J. Chem. Phys.* **2001**, *114*, 483–488.

- [35] Jackson, J. D. *Classical Electrodynamics*; Wiley: New York, 1975.
- [36] Dhirany, A.; Hines, A. J.; Fisher, A. J.; Ismail, O.; Guyot-Sionnest, P. *Langmuir* **1995**, *11*, 2609–2614.
- [37] Heinz, R.; Rabe, J. P. *Langmuir* **1995**, *11*, 506–511.
- [38] Fenter, P.; Eisenberger, P.; Li, J.; Camillone, N.; Bernasek, S.; Scoles, G.; Ramanarayanan, T. A.; Liang, K. S. *Langmuir* **1991**, *7*, 2013–2016.
- [39] Fonticelli, M.; Azzaroni, O.; Benitez, G.; Martins, M. E.; Carro, P.; Salvarezza, R. C. *J. Phys. Chem. B* **2004**, *108*, 1898–1905.
- [40] Yu, M.; Driver, S. M.; Woodruff, D. P. *Langmuir* **2005**, *21*, 7285.
- [41] Parkinson, G.; Hentz, A.; Quinn, P.; Window, A.; Woodruff, D.; Bailey, P.; Noakes, T. *Surf. Sci.* **2007**, *601*, 50–57.
- [42] Torres, D.; Carro, P.; Salvarezza, R. C.; Illas, F. *Phys. Rev. Lett.* **2006**, *97*, 226103.
- [43] Laibinis, P. E.; Whitesides, G. M.; Allara, D. L.; Tao, Y. T.; Parikh, A. N.; Nuzzo, R. G. *J. Am. Chem. Soc.* **1991**, *113*, 7152–7167.
- [44] Liu, G.-Y.; Fenter, P.; Chidsey, C. E. D.; Ogletree, D. F.; Eisenberger, P.; Salmeron, M. *J. Chem. Phys.* **1994**, *101*, 4301.
- [45] Alves, C. A.; Porter, M. D. *Langmuir* **1993**, *9*, 3507–3512.
- [46] Pflaum, J.; Bracco, G.; Schreiber, F.; Colorado, R.; Shmakova, O. E.; Lee, T. R.; Scoles, G.; Kahn, A. *Surf. Sci.* **2002**, *89*, 498.
- [47] Monreal, R. C.; Guillemot, L.; Esaulov, V. A. *J. Phys.: Condens. Matter.* **2003**, *15*, 1165–1171.
- [48] Bocquet, M. L.; Rappe, A. M.; Dai, H. L. *Mol. Phys.* **2005**, *103*, 883–890.